Bottom-up processing of thermoelectric nanocomposites from colloidal nanocrystal building blocks: the case of Ag2Te–PbTe

Doris Cadavid, Maria Ibáñez, Stéphane Gorsse, Antonio López, Albert Cirera, Joan Ramon Morante, Andreu Cabot

▶ **To cite this version:**

Doris Cadavid, Maria Ibáñez, Stéphane Gorsse, Antonio López, Albert Cirera, et al.. Bottom-up processing of thermoelectric nanocomposites from colloidal nanocrystal building blocks: the case of Ag2Te–PbTe. Journal of Nanoparticle Research, 2012, 14 (12), pp.1328. 10.1007/s11051-012-1328-0 . hal-04510058

HAL Id: hal-04510058
https://hal.science/hal-04510058

Submitted on 18 Mar 2024

HAL is a multi-disciplinary open access archive for the deposit and dissemination of scientific research documents, whether they are published or not. The documents may come from teaching and research institutions in France or abroad, or from public or private research centers.

L'archive ouverte pluridisciplinaire **HAL**, est destinée au dépôt et à la diffusion de documents scientifiques de niveau recherche, publiés ou non, émanant des établissements d'enseignement et de recherche français ou étrangers, des laboratoires publics ou privés.

Bottom-up processing of thermoelectric nanocomposites from colloidal nanocrystal building blocks: the case of Ag_2Te–PbTe

Doris Cadavid · Maria Ibáñez · Stéphane Gorsse · Antonio M. López · Albert Cirera · Joan Ramon Morante · Andreu Cabot

Keywords: Nanocomposites ; Colloidal nanoparticles ; Ag2Te ; PbTe ; Thermoelectric ; Energy ; Bottom-up

Abstract Nanocomposites are highly promising materials to enhance the efficiency of current thermoelectric devices. A straightforward and at the same time highly versatile and controllable approach to produce nanocomposites is the assembly of solution-processed nanocrystal building blocks. The convenience of this bottom-up approach to produce nanocomposites with homogeneous phase distributions and adjustable composition is demonstrated here by blending Ag_2Te and PbTe colloidal nanocrystals to form Ag_2Te–PbTe bulk nanocomposites. The thermoelectric properties of these nanocomposites are analyzed in the temperature range from 300 to 700 K. The evolution of their electrical conductivity and Seebeck coefficient is discussed in terms of the blend composition and the characteristics of the constituent materials.

D. Cadavid · J. R. Morante · A. Cabot (✉)
Catalonia Institute for Energy Research, IREC,
08930 Sant Adrià del Besos (Barcelona), Spain
e-mail: acabot@irec.cat

M. Ibáñez · A. Cirera · J. R. Morante · A. Cabot
Departament d'Electrònica, Universitat de Barcelona,
08028 Barcelona, Spain

S. Gorsse
CNRS, Université de Bordeaux, ICMCB, 87 avenue du
Docteur Albert Schweitzer, 33608 Pessac Cedex, France

A. M. López
Departament d'Enginyeria Electrónica, Universitat
Politècnica de Catalunya, EPSEVG, Av.Victor Balaguer
s/n, 08800 Barcelona, Spain

Introduction

Today's main strategy to engineer highly efficient thermoelectric materials is to reduce thermal conductivity by introducing phonon scattering centers at different length scales (Zebarjadi et al. 2012; Vineis et al. 2010). Alloys of heavy elements and complex solid solutions including 1D phonon scattering centers or 2D layered structures trigger phonon scattering at the atomic length scale (Dresselhaus et al. 2007; Gascoin et al. 2005; Feldman et al. 2000; Snyder and Toberer 2008). On the other hand, nanomaterials, having large interface densities introduced by the reduction of their crystal domains to the nanoscale, can efficiently scatter phonons at the 1–100 nm scale (Vaqueiro and Powell 2010; Bux et al. 2010; Szczech et al. 2011; Medlin and Snyder 2009; Poudel et al. 2008). A particularly interesting class of nanostruc-tured materials is that of nanocomposites containing crystal domains with different phases and/or compo-sitions. In nanocomposites, interfaces between dis-similar materials boost phonon scattering due to acoustic impedance mismatches (Cahill et al. 2003). Heterointerfaces may even allow reducing the electronic contribution to the thermal conductivity (Bian et al. 2007; Minnich et al. 2009; Humphrey and Linke

2005). Moreover, nanocomposites offer a mechanism to improve electrical conductivity through removing ionized impurities from avenues of charge carrier transport (Dingle et al. 1978; Zebarjadi et al. 2011). An additional potential advantage of nanocomposites is the possibility to decouple the Seebeck coefficient from electrical conductivity (Hicks and Dresselhaus 1993; Vashaee and Shakouri 2004; Sootsman et al. 2008). In this regard, the increase of the electronic density of states near the Fermi level in quantum confined nanostructures has been predicted to enhance the Seebeck coefficient (Szczech et al. 2011; Cornett and Rabin 2011). Additionally, energy filtering at nanocrystal interfaces may further enhance the thermopower of nanostructured material by selectively scattering low energy charge carriers (Heremans et al. 2004; Martin et al. 2009; Popescu et al. 2009; Faleev and Léonard 2008).

The ball-milling of crystalline ingots into fine powders and the posterior bulk reconstruction by hot-pressing is the most usual and general technique to obtain bulk nanocrystalline materials (Lan et al. 2010). However, such top–down industrial approach is time and energy consuming and no control on the size and shape of the nanoparticles is possible. The formation of nanoscale precipitates or organized superstructures by phase segregation in metastable solid solutions is a more elegant method to produce nanocomposites (Hsu et al. 2004; Quarez et al. 2005; Gorsse et al. 2010, 2011). Nevertheless, this procedure is limited to specific compositions and lacks of a high degree of control over the size and shape of the nanoinclusions.

Solution-synthesis routes are particularly well suited to provide nanoparticles for the bottom-up production of nanocomposites (Zhao et al. 2011; Scheele et al. 2009, 2010; Prasher 2006; Kovalenko et al. 2010; Ibáñez et al. 2013a, b) with a high degree of control over the size, shape, and composition of the crystal nanodomains (Ibáñez et al. 2011; Li et al. 2011). Nanocomposites can be easily obtained by simply mixing solutions containing different nanoparticles. Blending nanocrystals while dispersed in solution allows an intimate intermixing of the different components. After removal of organics, nanocrystals can be consolidated into macroscopic nanocomposites by techniques such as spark-plasma-sintering and cold- or hot-pressing. Even though the complete removal of surfactants is still a difficulty, important progress has also been achieved in this area (Scheele et al. 2010; Kovalenko et al. 2010). On the other hand, self-purification allows the use of relatively low purity precursors, which is economically advantageous. However, it hampers the potential for nanocrystal doping (Dalpian and Chelikowsky 2006; Norris et al. 2008; Erwin et al. 2005). This drawback can be overcome by adjusting the composition in ternary or quaternary compounds (Ibáñez et al. 2012a, b, c). Another possibility to control carrier concentration in nanocomposites obtained by bottom-up approaches is to cleverly select the combination of materials and their correct proportions (Urban et al. 2007; Ko et al. 2010).

An especially appealing thermoelectric nanomaterial is the one obtained from the combination of lead and silver tellurides (Lensch-Falk et al. 2010; Pei et al. 2011a, b; Paul et al. 2010). The control of the carrier concentration and the formation of nanocrystalline inclusions in these nanocomposites have allowed reaching ZT values up to 1.6 (Pei et al. 2011a, b).

The present work explores the potential of solution-processing techniques to obtain binary bulk nanocomposites with superior thermoelectric properties in the system Ag-Pb-Te. Binary Ag_2Te–PbTe bulk nanocomposites were produced by blending in solution PbTe and Ag_2Te nanocrystals in different proportions. The thermoelectric properties of the formed nanocomposites were analyzed in the temperature range from 300 to 700 K.

Experimental details

Materials

Tri-n-octylphosphine (TOP, 97 %) and silver chloride (99.9 %) were purchased from Strem. Tellurium pieces (99.999 %), lead acetate trihydrate (99.999 %), 1-octadecene (ODE, 90 %), oleylamine (OLA tech. 70 %), and oleic acid (OA, tech. 90 %) were purchased from Aldrich. Analytical grade ethanol, hexane, and toluene were purchased from Panreac. All chemicals were used without further purifications. Stock solutions of TOP-Te (1 M) and TOP-Ag (1 M) were prepared by dissolving 12.76 g of tellurium pieces and 14.33 g of silver chloride in 100 ml of TOP, respectively. These solutions were prepared and stored inside an Ar-filled glovebox.

All nanocrystal preparations were carried out using standard airless techniques: a vacuum/dry Ar Schlenk line was used for the synthesis and an Ar-filled

glovebox for storing and handling air- and moisture-sensitive chemicals.

Preparation of PbTe nanocrystals

A modified approach of that used by Urban et al. (2006) was used for the preparation of PbTe nanocrystals. In a typical procedure, lead acetate tryhidrate (0.5670 g, 1.5 mM) and OA (1.5 ml, 4.75 mM) were dissolved in 10 ml ODE. This mixture was degassed at 70 and 150 °C for 0.5 h to form lead oleate complex and remove water and acetic acid. The solution was flushed with Ar and the temperature was raised up to 180 °C. Afterward, 2 ml of 1 M TOP-Te were rapidly injected. The reaction mixture was maintained in the temperature range 160–180 °C for 3 min and then quickly cooled down to room temperature using a water bath. After cooling, the nanoparticles were precipitated by adding a hexane/ethanol (3:1) combination followed by centrifugation. This procedure was repeated twice. The precipitated nanoparticles were transferred to an Ar-filled glovebox, where they were stored until future use.

Preparation of Ag_2Te nanocrystals

Ag_2Te nanocrystals were produced using a modified version of the method developed by Ko et al. (2010). In a typical procedure, 10 ml of OLA were added to a three-neck flask and heated up to 100 °C under vacuum for 1 h to remove low boiling point impurities and water. Afterward, the reaction flask was flushed with Ar and temperature was raised up to 160 °C. A mixture of 5 ml of TOP-Ag stock solution and 2.5 ml of TOP-Ag was quickly injected. After injection, the reaction temperature was maintained between 130 and 160 °C for 3 min. Then the reaction solution was cooled using a cold water bath. Ag_2Te nanocrystals were precipitated and redispersed using ethanol and toluene twice. Finally, the nanocrystals were dispersed in toluene and stored in the glovebox.

Nanocomposite preparation

PbTe and Ag_2Te nanoparticles dispersed in toluene were blended at various molar fractions, 25/75, 50/50, and 75/25. After several additional precipitation and redispersion cycles, the resultant blends were dried under Ar atmosphere. The blends were annealed at 500 °C during 2 h in Ar flow. Finally, the resulting materials were pressed under a load of 5 tons at room temperature. This way, dense pellets with 13 mm diameter and 1 mm thickness were obtained.

Structural and chemical characterization

Powder X-ray diffraction (XRD) analysis were carried out on a Bruker AXS D8 ADVANCE X-ray diffractometer with Cu Kα1 radiation ($\lambda = 1.5406$ Å). Size and shape of the nanoparticles were examined by transmission electron microscopy (TEM) using a JEOL 2100 operating at 200 keV accelerating voltage. Scanning electron microscopy (SEM) was performed using a ZEISS Auriga SEM with an energy-dispersive X-ray spectroscopy (EDX) detector to study composition. X-ray photoelectron spectroscopy (XPS) spectra were obtained using a *SPECS SAGE ESCA* System employing Mg Kα ($E = 1{,}253.6$ eV) with a supplied power of 203 W as the X-ray source.

Thermoelectric characterization

Seebeck coefficient and electrical resistivity were measured simultaneously using a Linseis—LSR 3 system under helium atmosphere. The Seebeck coefficient was obtained using a static DC method. The electrical resistivity was measured by means of a standard four probe technique in the temperature range from 300 to 700 K. Thermal conductivity measurements were obtained from flash diffusivity measurements (Netzsch LFA-457 Microflash) using the mass density and the Dulong-Petit approximation to determine the specific heat capacity. The thermal conductivity was calculated as $\kappa = DC_p d$, where D is the thermal diffusivity, C_p is the heat capacity, and d is the density.

Results and discussion

Figure 1 shows representative TEM micrographs of the PbTe and Ag_2Te nanoparticles used as building blocks to produce the $(Ag_2Te)_x(PbTe)_{1-x}$ ($x = 0.25$, 0.50, 0.75) nanocomposites. Insets display the histograms of their size distribution. PbTe nanoparticles had cubic morphologies and a face-centered cubic crystal phase (JCPDS 38-1435). Their average size, taken as the diagonal of one of their faces was 19 nm

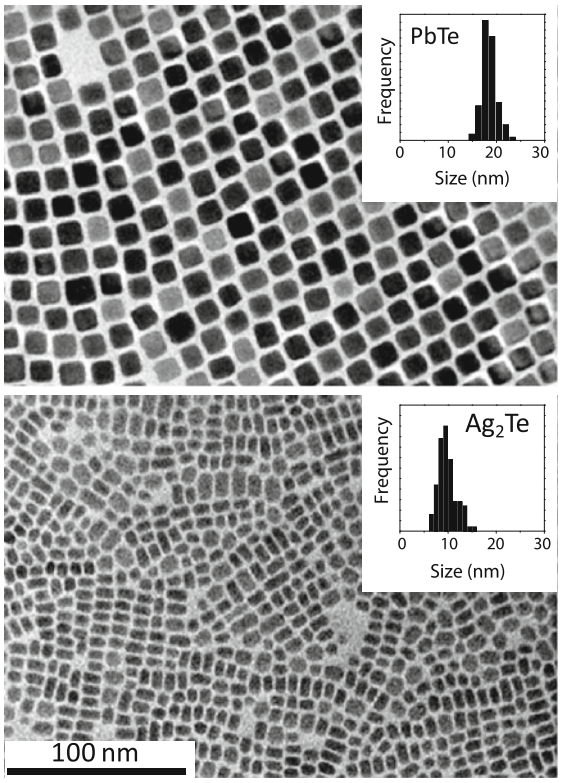

Fig. 1 Representative TEM micrographs of the PbTe (*top*) and Ag_2Te (*bottom*) nanoparticles used to produce the nanocomposites. *Insets* display the histograms of the particle size distributions

and their size distribution had 5 % dispersion. Ag_2Te nanoparticles had disk-like morphology and a monoclinic crystal phase at ambient temperature (JCPDS 34-0142). Their average diameter was 10 nm and their size dispersion was close to 10 %. PbTe and Ag_2Te nanoparticles were not intentionally doped by extrinsic impurities.

Figure 2 shows a scheme of the procedure used to produce the binary nanocomposites from solutions containing the PbTe and Ag_2Te colloidal building blocks. While short range ordering of the nanocrystals at submicron scales may exist, at the macroscopic level the different phases must be considered as randomly distributed. The nanoparticle mixture was prepared while having the nanocrystals well dispersed in toluene to ensure a homogeneous blending of the two components at the nanometer scale. Three different compositions were prepared, having the following molar fractions: $(Ag_2Te)_{0.75}(PbTe)_{0.25}$, $(Ag_2Te)_{0.50}(PbTe)_{0.50}$, and $(Ag_2Te)_{0.25}(PbTe)_{0.75}$. Once mixed, the nanoparticle blends were thoroughly purified by multiple precipitation and redispersion steps. Final nanoparticles were not soluble, probing the high degree of surfactant removal from their surfaces. The purified nanoparticle blends were annealed at 500 °C during 2 h in an argon flow atmosphere. The concentration of residual carbon in the final materials was less than 2 %, as determined by elemental analysis. The annealed nanocomposite powders were cold-pressed into 13 mm pellets by applying 380 MPa pressure with a hydraulic press. At the same time, pure Ag_2Te and PbTe pellets were prepared following the same protocol and using the exact same nanocrystals used to obtain the blends. The relative density of the produced pellets was around 80 %. Figure 3 shows a SEM image of the $(Ag_2Te)_{0.75}(PbTe)_{0.25}$ nanopowders obtained after annealing. Elemental mappings obtained by SEM-EDX characterization of the nanocomposites showed the spatial distribution of the two phases to be highly homogeneous (Fig. 3).

Figure 4 shows the XRD patterns of the annealed nanomaterials. The XRD patterns of the nanocomposites resembled the combination of the XRD patterns obtained from the pure materials. No evidences of alloying between the two phases could be obtained from this analysis. At the same time, no secondary phases were detected. The fitting of the XRD patterns allowed estimating the growth of the crystallographic domains with the thermal treatment. From the Scherer equation, the crystal domain size of both phases in the annealed material was calculated to be approximately 40 nm.

XPS analysis of the materials revealed an increase of the oxygen concentration at the nanoparticle surface with the annealing treatment. Typically, XPS analysis of the nanoparticle before annealing (but exposed to air for several hours) showed a 7 % concentration of oxygen. This value increased up to a 30 % with the annealing process. Therefore, we estimate oxidation to extend 1–2 nm from the particle surface, forming an amorphous oxide shell.

The electrical conductivity and Seebeck coefficient of the nanocomposites were characterized in the temperature range from 300 to 700 K. Figure 5(left) and (center) display the temperature dependence of the electrical conductivity and Seebeck coefficient for the three $(Ag_2Te)_x(PbTe)_{1-x}$ ($x = 0.25, 0.50, 0.75$) nanocomposites and for the pure PbTe and Ag_2Te nanomaterials.

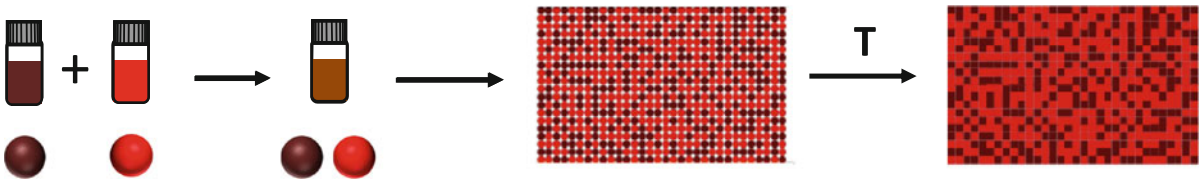

Fig. 2 Scheme of the procedure used to produce binary nanocomposites from solution-processed nanocrystals

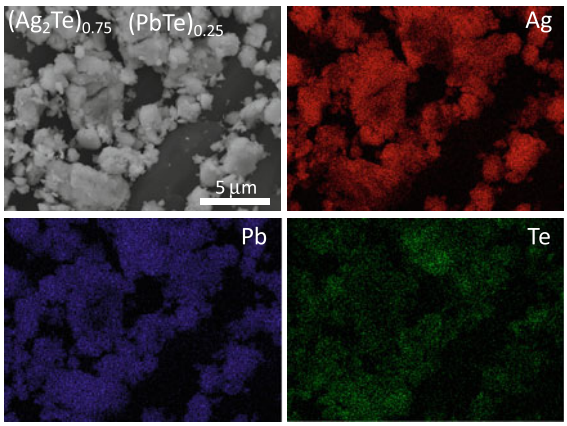

Fig. 3 SEM image and EDX elemental maps of the annealed $(Ag_2Te)_{0.75}$ $(PbTe)_{0.25}$ nanocomposite powder

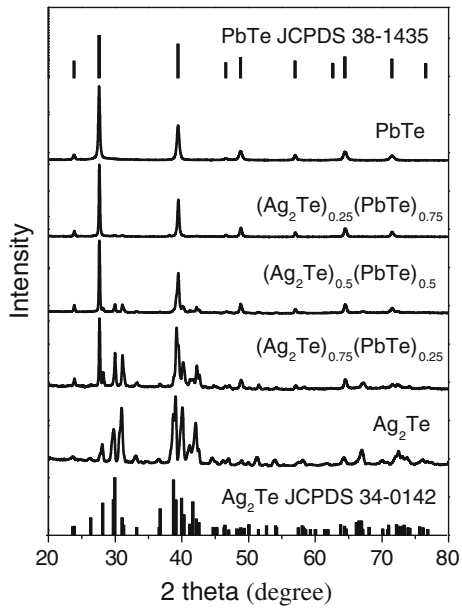

Fig. 4 XRD patterns of the annealed nanocomposites. Ag_2Te (JCPDS 34-0142) and PbTe (JCPDS 38-1435) patterns have been included as a reference

One first clearly noticeable feature in Fig. 5(left) is the non-monotonic evolution of the pure Ag_2Te electrical conductivity with temperature. For this material, a decrease of electrical conductivity of over an order of magnitude was systematically obtained in the temperature range between 400 and 450 K. This is associated to the well-known phase transition from the low-temperature monoclinic α-Ag_2Te to the high-temperature cubic β-Ag_2Te.[1] The low-temperature α-Ag_2Te phase is a very narrow band-gap semiconductor ($E_g = 0.025$ eV), which in bulk displays high electron mobility and a low lattice thermal conductivity (Sakuma and Saitoh 1985; Fujikane et al. 2005a, b; Taylor and Wood 1961; Capps et al. 2010; Dalven and Gill 1966; Wood et al. 1961; Schneider and Schulz 1993; Dalven and Gill 1967). A slight decrease of electrical conductivity with temperature and a negative Seebeck coefficient in the range 300–400 K were measured for this material. These results are consistent with previous reports showing the low-temperature α-Ag_2Te to be a degenerate semiconductor displaying n-type conductivity (Das and Karunakaran 1984). Our experimental results showed the phase transformation for this material to be accompanied by a transition from n-type to p-type conductivity. The high-temperature β-Ag_2Te bulk nanomaterial displayed a positive Seebeck coefficient and its electrical conductivity increased with temperature in all the range measured. In intrinsic β-Ag_2Te, the much lower effective masses for electrons than holes usually translate into an n-type conductivity (Fujikane et al. 2005a, b). However, the conductivity type of this material is known to be highly dependent on composition. In this regards, stoichiometric and Ag-rich samples show n-type conductivity, while Te-rich Ag_2Te displays p-type conductivity (Capps et al. 2011; Max-Planck-Gesellschaft 1973). Aside from composition variations, the p-type conductivity obtained here could be explained by a possible surface oxidation of the small colloidal nanocrystals during their processing into pellets. From

[1] Notice that there is some controversy in the nomenclature of the different Ag_2Te phases. We use α to denote the low-temperature Ag_2Te phase and β for the high-temperature one.

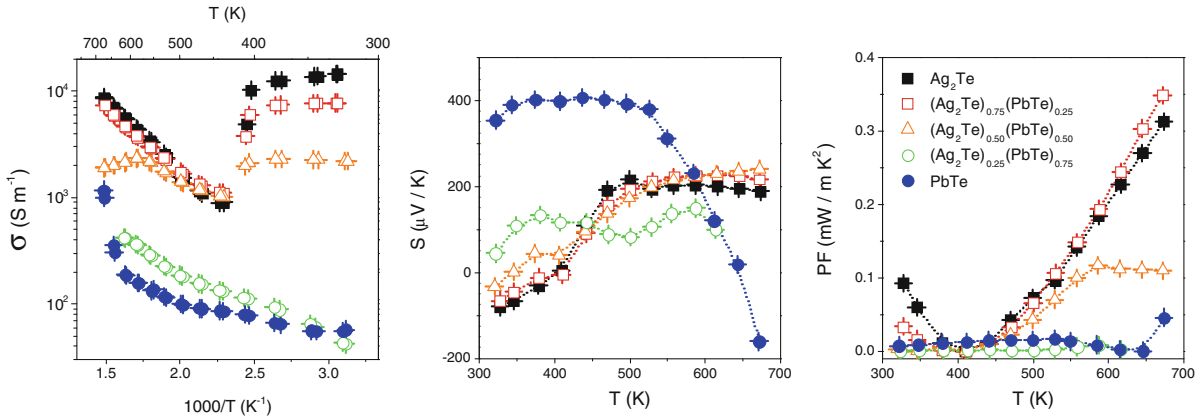

Fig. 5 Temperature dependence of the electrical conductivity (*left*), Seebeck coefficient (*center*), and power factor (*right*) obtained from the produced nanomaterials: Ag_2Te (*filled square*); $(Ag_2Te)_{0.75}(PbTe)_{0.25}$ (*open square*); $(Ag_2Te)_{0.5}(PbTe)_{0.5}$ (*open triangle*); $(Ag_2Te)_{0.25}(PbTe)_{0.75}$ (*open circle*); PbTe (*filled circle*)

the lineal dependence of $\ln \sigma T^{-3/2}$ with the inverse of temperature in the high-temperature range, an activation energy for electrical conductivity of 0.18 eV was calculated. This activation energy could be associated with the thermal generation of electron-hole pairs through a 0.36 eV band gap. The flattening of the Seebeck coefficient evolution with the temperature supports the hypothesis of an intrinsic semiconductor character at this high-temperature region. However, the obtained band gap is considerably higher than the 0.20–0.28 eV measured previously for this material (Van Dong and Tung 1968). From the maximum of the Seebeck coefficient obtained for this material and using the equation $E_g = 2eS_{max}T_{max}$ (Goldsmid and Sharp 1999), a 0.2 eV band gap was calculated. This value is consistent with previously published band gap estimates. Thus, the calculated activation energy for electrical conductivity should be at least in part associated with mobility energy barriers at the grain boundaries, which probably results from the presence of an oxide layer at the nanoparticles surface (Ko et al. 2010; Scheele et al. 2011).

Pure PbTe pellets displayed p-type electrical conductivity in most of the temperature range measured. The p-type character of the PbTe nanocrystalline pellet had its origin on a thin oxide layer at the nanoparticles surface (Paul and Banerji 2011; Rogacheva et al. 2001; Schenk et al. 1988; Wang et al. 2008), on the presence of electrically active lattice defects associated with deviations from stoichiometry or on the broken bonds at the grain boundaries (Borisova 1979; Breschi et al. 1982; Crocker and Rogers 1967; Martin et al. 2007; Allgaier 1961; Grekov et al. 1997; Scanlon 1962; Dashevsky et al. 2005). The slight increase of electrical conductivity with temperature in the low temperature range and the constant Seebeck coefficient obtained pointed toward the full ionization of acceptor levels at temperatures above 350 K. From the maximum of the Seebeck coefficient, a 0.30 eV band gap was calculated. This value correlated well with the optical band gap previously measured for this material (Zemel et al. 1965). A sign inversion in the carrier type, from p to n, was clearly observed at approximately 650 K. This was probably associated with the thermal activation of electron-hole pairs through the semiconductor band gap. The higher mobilities for electrons than holes in this material would compensate the higher hole concentration and trigger the conduction type inversion. The conduction type inversion was accompanied by a strong increase of electrical conductivity above 600 K, most probably associated to the overcome of the energy barriers at the grain boundaries.

In the low-temperature range, the blending of Ag_2Te with PbTe nanocrystals resulted in nanocomposites with electrical conductivities lower than that of Ag_2Te. This electrical conductivity decrease was associated with a reduction of the charge carrier mobility with the blending, or with a reduction of the charge carrier density with the reduction of the relative Ag_2Te content. A partial compensation of the majority carriers of each material may also contribute to the lower electrical conductivities observed. Below the Ag_2Te phase transition temperature, a shift of the

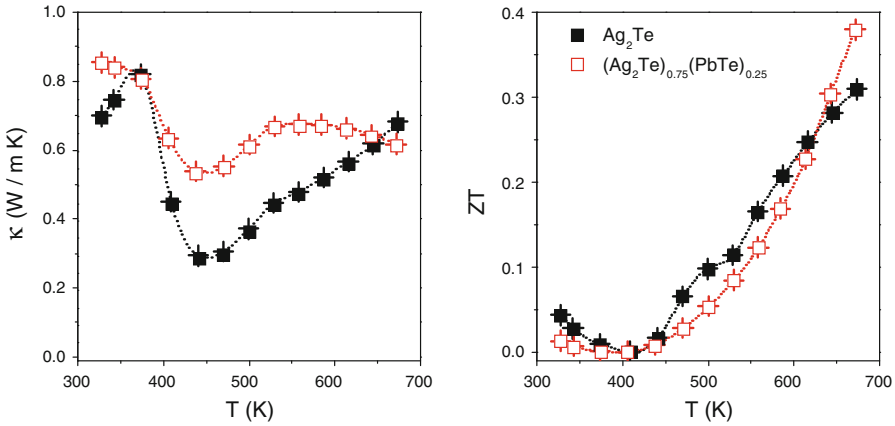

Fig. 6 Temperature dependence of the thermal conductivity (*left*) and thermoelectric figure of merit (*right*) obtained from the $(Ag_2Te)_{0.75}(PbTe)_{0.25}$ nanocomposite (*open square*) and the Ag_2Te nanomaterial (*filled square*)

Seebeck coefficient toward positive values was also obtained when increasing the PbTe ratio in the blend.

In the full temperature range, the temperature dependences of the electrical conductivities and Seebeck coefficients obtained with the $(Ag_2Te)_{0.75}(PbTe)_{0.25}$ and $(Ag_2Te)_{0.5}(PbTe)_{0.5}$ nanocomposites clearly resembled that of pure Ag_2Te. In these two nanocomposites, a step change in the conductivity and the Seebeck coefficient was also observed at around 420 K. This was associated with the monoclinic to cubic phase transition taking place within the Ag_2Te crystallographic domains. Like in the case of pure Ag_2Te, in the low temperature range, nanocomposites showed n-type conductivity with a minor temperature dependence of the conductivity. On the other hand, above 450 K, nanocomposites displayed p-type character and a clear increase of electrical conductivity with temperature. In both nanocomposites, an activation energy for conductivity similar to that obtained for pure Ag_2Te material could be observed. However, in the 50 % blend, a clear influence of PbTe was obtained above 600 K, where a decrease of electrical conductivity was obtained. This was most probably related with the recombination of the n-type carriers created within the PbTe nanocrystals with the majoritary holes within the Ag_2Te. This decrease of electrical conductivity resulted in a limitation of this material's power factor above 600 K, as shown in Fig. 5.

The temperature dependence of the electrical conductivity measured from the $(Ag_2Te)_{0.25}(PbTe)_{0.75}$ nanocomposite resembled that of the pure PbTe nanomaterial. It showed a monotone increase with the temperature. Different lineal regions were observed when plotting the logarithm of conductance against reciprocal temperature, revealing the existence of multiple energy activated barriers and thus the contribution of multiple acceptor and donor states to charge transport.

Nanocomposites were characterized by temperature dependences of the electrical conductivity and Seebeck coefficient that clearly resembled those of the pure materials. This fact pointed toward the coexistence of the two phases within the nanocomposite, which was consistent with the results obtained from the XRD characterization of the materials. The alloying of the two materials would be expected to result in a modification of the semiconductor band gap and thus into different dependences of the thermoelectric properties with temperature (Pei et al. 2011a, b).

The best power factors were finally obtained from the pure Ag_2Te nanomaterial and the $(Ag_2Te)_{0.75}(PbTe)_{0.25}$ nanocomposites. For these two materials, the thermal conductivity was also measured (Fig. 6). A clear decrease of the thermal conductivity with the low temperature monoclinic α-Ag_2Te to the high-temperature cubic β-Ag_2Te phase transition was noticed at around 400 K. The already very low thermal conductivities obtained for the pure Ag_2Te nanomaterial hinder a further decrease of thermal conductivity with the blending of the two different phases. Only in the high-temperature range, the nanocomposite displayed lower thermal conductivities than the pure material. The low thermal conductivities obtained for both samples in all the temperature range measured are related to the very high density of interfaces and the relatively low density of the pellets measured. Higher pellet densities would have associated both a higher thermal conductivity and a higher electrical conductivity. This effect was estimated to

account for up to a 40 % variation of both thermal and electric conductivity of the theoretical value to be expected for sample with 100 % relative density (Scheele et al. 2010).

The thermoelectric figure of merit reached up to 0.38 for the $(Ag_2Te)_{0.75}(PbTe)_{0.25}$ nanocomposite at 670 K (Fig. 6). This represents a 25 % increase over pure Ag_2Te and it is an excellent ZT value taking into account that no extrinsic doping was intentionally introduced in these materials. The production of nanocomposites with much higher thermoelectric figures of merit ($ZT > 1.5$) by bottom-up approaches based on solution-processed nanocrystals will necessarily require the control of the carrier concentration of each compound through doping.

Conclusion

$(Ag_2Te)_x(PbTe)_{1-x}$ nanocomposites with controlled composition were obtained by means of a very facile bottom-up approach consisting in the solution blending of colloidal nanocrystals. The temperature dependence of the electrical conductivity and Seebeck coefficient of the obtained materials could be described from the combination of the properties of the two constituent materials. Undoped $(Ag_2Te)_{0.75}(PbTe)_{0.25}$ nanocomposites displayed the best power factors among the different nanocomposites tested and reached ZT values up to 0.38 at 670 K.

Acknowledgments The research was supported by the European Regional Development Funds and the Spanish MICINN Projects MAT2008-05779, MAT2008-03400-E/MAT, MAT2010-15138, MAT2010-21510, CSD2009-00050, and ENE2008-03277-E/CON. M.I. is grateful to the Spanish MICINN for her PhD grant. A. Cirera acknowledges support from ICREA Academia program. A. Cabot is grateful to the Spanish MICINN for financial support through the Ramón y Cajal program.

References

Allgaier RS (1961) Valence bands in lead telluride. J Appl Phys 32:2185–2189

Bian Z, Zebarjadi M, Singh R et al (2007) Cross-plane Seebeck coefficient and Lorenz number in superlattices. Phys Rev B 76:205311

Borisova LD (1979) Thermoelectric properties of impurity doped PbTe. Physica Status Solidi (a) 53:K19–K22

Breschi R, Camanzi A, Fano V (1982) Defects in PbTe single crystals. J Cryst Growth 58:399–408

Bux SK, Fleurial J-P, Kaner RB (2010) Nanostructures materials for thermoelectric applications. Chem Comm 46:8311–8324

Cahill DG, Ford WK, Goodson KE et al (2003) Nanoscale thermal transport. J Appl Phys 93:793–818

Capps J, Drymiotis F, Lindsey S, Tritt TM (2010) Significant enhanced of the dimensionless thermoelectric figure of merit binary Ag_2Te. Phyl Mag Lett 90:677–681

Capps J, Ma B, Drye T et al (2011) The effect of Ag concentration on the structural, electrical and thermal transport behavior of Pb:Te:Ag:Se mixtures and improvement of thermoelectric performance via Cu doping. J Alloy Compd 509:1544–1549

Cornett JE, Rabin O (2011) Thermoelectric figure of merit calculations for semiconducting nanowires. Appl Phys Lett 98:182104–182104–3

Crocker AJ, Rogers LM (1967) Interpretation of the Hall coefficient, electrical resistivity and Seebeck coefficient of p-type lead telluride. Br J Appl Phys 18:563–573

Dalpian GM, Chelikowsky JR (2006) Self-purification in semiconductor nanocrystals. Phys Rev Lett 96:226802

Dalven R, Gill R (1966) Energy gap in β-Ag_2Te. Phys Rev 143:666–670

Dalven R, Gill R (1967) Electrical properties of β-Ag_2Te and β-Ag_2Se from 4.2° to 300°K. J Appl Phys 38:753–756

Das VD, Karunakaran D (1984) Thermoelectric studies on semiconducting Ag_2Te thin films: temperature and dimensional effects. Phys Rev B 30:2036–2041

Dashevsky Z, Kreizman R, Dariel MP (2005) Physical properties and inversion of conductivity type in nanocrystalline PbTe films. J Appl Phys 98:094309–094309–5

Dingle R, Störmer HL, Gossard AC, Wiegmann W (1978) Electron mobilities in modulation-doped semiconductor heterojunction superlattices. Appl Phys Lett 33:665–667

Dresselhaus MS, Chen G, Tang MY et al (2007) New directions for low-dimensional thermoelectric materials. Adv Mater 19:1043–1053

Erwin SC, Zu L, Haftel MI et al (2005) Doping semiconductor nanocrystals. Nature 436:91–94

Faleev SV, Léonard F (2008) Theory of enhancement of thermoelectric properties of materials with nanoinclusions. Phys Rev B 77:214304

Feldman JL, Singh DJ, Mazin II, Mandrus D, Sales BC (2000) Lattice dynamics and reduced thermal conductivity of filled skutterudites. Phys Rev B 61:R9209–R9212

Fujikane M, Kurosaki K, Muta H, Yamanaka S (2005a) Thermoelectric properties of α- and β-Ag_2Te. J Alloy Compd 393:299–301

Fujikane M, Kurosaki K, Muta H, Yamanaka S (2005b) Electrical properties of α- and β-Ag_2Te. J Alloy Compd 387: 297–299

Gascoin F, Ottensmann S, Stark D, Haile SM, Snyder GJ (2005) Zintl phases as thermoelectric materials: tuned transport properties of the compounds $Ca_xYb_{1-x}Zn_2Sb_2$. Adv Funct Mater 15:1860–1864

Goldsmid H, Sharp J (1999) Estimation of the thermal band gap of a semiconductor from seebeck measurements. J Electron Mater 28:869–872

Gorsse S, Bauer Pereira P, Decourt R, Sellier E (2010) Microstructure engineering design for thermoelectric materials: an approach to minimize thermal diffusivity. Chem Mater 22:988–993

Gorsse S, Bellanger P, Brechet Y, Sellier E, Umarji A, Ail U, Decourt R (2011) Nanostructuration via solid state transformation as a strategy for improving the thermoelectric efficiency of PbTe alloys. Acta Mater 59:7425–7437

Grekov Y, Shlyakhov T, Semikolenova N (1997) Inversion of the conduction type of epitaxial films of PbSnTe solid solutions under the influence of laser irradiation at subthreshold power. Semiconductors 31:844–846

Heremans JP, Thrush CM, Morelli DT (2004) Thermopower enhancement in lead telluride nanostructures. Phys Rev B 70:115334

Hicks LD, Dresselhaus MS (1993) Effect of quantum-well structures on the thermoelectric figure of merit. Phys Rev B 47:12727–12731

Hsu KF, Loo S, Guo F et al (2004) Cubic AgPbmSbTe2+m: bulk thermoelectric materials with high figure of merit. Science 303:818–821

Humphrey TE, Linke H (2005) Reversible thermoelectric nanomaterials. Phys Rev Lett 94:096601

Ibáñez M, Guardia P, Shavel A et al (2011) Growth kinetics of asymmetric Bi2S3 nanocrystals: size distribution focusing in nanorods. J Phys Chem C 115:7947–7955

Ibáñez M, Cadavid D, Zamani R et al (2012a) Composition control and thermoelectric properties of quaternary chalcogenide nanocrystals: the case of stannite Cu2CdSnSe4. Chem Mater 24:562–570

Ibáñez M, Zamani R, LaLonde A et al (2012b) Cu2ZnGeSe4 nanocrystals: synthesis and thermoelectric properties. J Am Chem Soc 134:4060–4063

Ibáñez M, Zamani R, Li W, Shavel A, Arbiol J, Morante JR, Cabot A (2012c) Extending the nanocrystal synthesis control to quaternary compositions. Cryst Growth Des 12:1085–1090

Ibáñez M, Zamani R, Li W et al (2013a) Chem Mater. doi: 10.1021/cm303252q

Ibáñez M, Cadavid D, Anselmi-Tamburini U et al (2013b) J Mater Chem A. doi:10.1039/c2ta00419d

Ko D-K, Urban JJ, Murray CB (2010) Carrier distribution and dynamics of nanocrystal solids doped with artificial atoms. Nano Lett 10:1842–1847

Kovalenko MV, Spokoyny B, Lee J-S et al (2010) Semiconductor nanocrystals functionalized with antimony telluride zintl ions for nanostructured thermoelectrics. J Am Chem Soc 132:6686–6695

Lan Y, Minnich AJ, Chen G, Ren Z (2010) Enhancement of thermoelectric figure-of-merit by a bulk nanostructuring approach. Adv Funct Mater 20:357–376

Lensch-Falk JL, Sugar JD, Hekmaty MA, Medlin DL (2010) Morphological evolution of Ag_2Te precipitates in thermoelectric PbTe. J Alloy Compd 504:37–44

Li W, Shavel A, Guzman R et al (2011) Morphology evolution of Cu2 − xS nanoparticles: from spheres to dodecahedrons. Chem Commun 47:10332

Martin J, Nolas GS, Zhang W, Chen L (2007) PbTe nanocomposites synthesized from PbTe nanocrystals. Appl Phys Lett 90:222112

Martin J, Wang L, Chen L, Nolas GS (2009) Enhanced Seebeck coefficient through energy-barrier scattering in PbTe nanocomposites. Phys Rev B 79:115311

Max-Planck-Gesellschaft zur Förderung der Wissenschaften (1973) Gmelin Handbuch der anorganischen Chemie, 8. völlig neu bearbeitete Aufl. Springer, Berlin

Medlin DL, Snyder GJ (2009) Interfaces in bulk thermoelectric materials: a review for current opinion in colloid and interface science. Curr Opin Colloid Interface Sci 14:226–235

Minnich AJ, Dresselhaus MS, Ren ZF, Chen G (2009) Bulk nanostructured thermoelectric materials: current research and future prospects. Energy Environ Sci 2:466–479

Norris DJ, Efros AL, Erwin SC (2008) Doped nanocrystals. Science 319:1776–1779

Paul B, Banerji PJ (2011) Enhancement in thermoelectric power in lead telluride nanocomposite: role of oxygen vis-à-vis nanostruct. Nano Electron Phys 3:691–697

Paul B, Kumar VA, Banerji P (2010) Embedded Ag-rich nanodots in PbTe: enhancement of thermoelectric properties through energy filtering of the carriers. J Appl Phys 108:064322

Pei Y, Heinz NA, Snyder GJ (2011a) Alloying to increase the band gap for improving thermoelectric properties of Ag_2Te. J Mater Chem 21:18256

Pei Y, Lensch-Falk J, Toberer ES, Medlin DL, Snyder GJ (2011b) High thermoelectric performance in PbTe due to large nanoscale Ag_2Te precipitates and La doping. Adv Funct Mater 21:241–249

Popescu A, Woods LM, Martin J, Nolas GS (2009) Model of transport properties of thermoelectric nanocomposite materials. Phys Rev B 79:205302

Poudel B, Hao Q, Ma Y et al (2008) High-thermoelectric performance of nanostructured bismuth antimony telluride bulk alloys. Science 320:634–638

Prasher R (2006) Ultralow thermal conductivity of a packed bed of crystalline nanoparticles: a theoretical study. Phys Rev B 74:165413

Quarez E, Hsu K-F, Pcionek R, Frangis N, Polychroniadis EK, Kanatzidis MG (2005) Nanostructuring compositional fluctuations and atomic ordering in the thermoelectric materials $AgPb_mSbTe_{2+m}$ the myth of solid solutions. J Am Chem Soc 127:9177–9190

Rogacheva EI, Krivulkin IM, Nashchekina ON, Sipatov AYu, Volobuev VV, Dresselhaus MS (2001) Effect of oxidation on the thermoelectric properties of PbTe and PbS epitaxial films. Appl Phys Lett 78:1661–1663

Sakuma T, Saitoh S (1985) Structure of α-Ag_2Te. J Phys Soc Jpn 54:3647–3648

Scanlon W (1962) Precipitation of Te and Pb in PbTe crystals. Phys Rev 126:509–513

Scheele M, Oeschler N, Meier K, Kornowski A, Klinke C, Weller H (2009) Synthesis and thermoelectric characterization of Bi_2Te_3 nanoparticles. Adv Funct Mater 19:3476–3483

Scheele M, Oeschler N, Veremchuk I, Reinsberg K-G, Kreuziger A-M, Kornowski A, Broekaert J, Klinke C, Weller H (2010) ZT enhancement in solution-grown $Sb_{(2-x)}Bi_xTe_3$ nanoplates. ACS Nano 4:4283–4291

Scheele M, Oeschler N, Veremchuk I et al (2011) Thermoelectric properties of lead chalcogenide core–shell nanostructures. ACS Nano 5:8541–8551

Schenk M, Berger H, Klimakow A, Mühlberg M, Wienecke M (1988) Nonstoichiometry and point defects in PbTe. Cryst Res Technol 23:77–84

Schneider J, Schulz H (1993) X-ray powder diffraction of Ag_2Te at temperatures up to 1123 K. Z Kristallogr 203: 1–15

Snyder GJ, Toberer ES (2008) Complex thermoelectric materials. Nat Mater 7:105–114

Sootsman JR, Kong H, Uher C et al (2008) Large enhancements in the thermoelectric power factor of bulk PbTe at high temperature by synergistic nanostructuring. Angew Chem 120:8746–8750

Szczech JR, Higgins JM, Jin S (2011) Enhancement of the thermoelectric properties in nanoscale and nanostructured materials. J Mater Chem 21:4037–4055

Taylor PF, Wood C (1961) Thermoelectric properties of Ag_2Te. J Appl Phys 32:1–3

Urban JJ, Talapin DV, Shevchenko EV, Murray CB (2006) Self-assembly of PbTe quantum dots into nanocrystal superlattices and glassy films. J Am Chem Soc 128:3248–3255

Urban JJ, Talapin DV, Shevchenko EV et al (2007) Synergism in binary nanocrystal superlattices leads to enhanced p-type conductivity in self-assembled PbTe/Ag_2Te thin films. Nat Mater 6:115–121

Van Dong N, Tung PN (1968) Transport properties of silver telluride in the solid and liquid states. Physica status solidi (b) 30:557–567

Vaqueiro P, Powell AV (2010) Recent developments in nanostructured materials for high-performance thermoelectrics. J Mater Chem 20:9577

Vashaee D, Shakouri A (2004) Improved thermoelectric power factor in metal-based superlattices. Phys Rev Lett 92: 106103

Vineis CJ, Shakouri A, Majumdar A, Kanatzidis MG (2010) Nanostructured thermoelectrics: big efficiency gains from small features. Adv Mater 22:3970–3980

Wang RY, Feser JP, Lee J-S et al (2008) Enhanced thermopower in PbSe nanocrystal quantum dot superlattices. Nano Lett 8:2283–2288

Wood C, Harrap V, Kane WM (1961) Degeneracy in Ag_2Te. Phys Rev 121:978–982

Zebarjadi M, Joshi G, Zhu G et al (2011) Power factor enhancement by modulation doping in bulk nanocomposites. Nano Lett 11:2225–2230

Zebarjadi M, Esfarjani K, Dresselhaus MS et al (2012) Perspectives on thermoelectrics: from fundamentals to device applications. Energy Environ Sci 5:5147

Zemel JN, Jensen JD, Schoolar RB (1965) Electrical and optical properties of epitaxial films of PbS, PbSe, PbTe, and SnTe. Phys Rev 140:A330–A342

Zhao Y, Dyck JS, Burda C (2011) Toward high-performance nanostructured thermoelectric materials: the progress of bottom-up solution chemistry approaches. J Mater Chem 21:17049